Read-out of single spins by optical spectroscopy

2004 J. Phys.: Condens. Matter 16 R1089

(http://iopscience.iop.org/0953-8984/16/30/R03)

INSTITUTE OF PHYSICS PUBLISHING JOURNAL OF PHYSICS: CONDENSED MATTER

J. Phys.: Condens. Matter **16** (2004) R1089–R1104 PII: S0953-8984(04)59361-X

TOPICAL REVIEW

Read-out of single spins by optical spectroscopy

F Jelezko and J Wrachtrup

3. Physical Institute, University of Stuttgart, Stuttgart 70550, Germany

Received 20 January 2004
Published 16 July 2004
Online at stacks.iop.org/JPhysCM/16/R1089
doi:10.1088/0953-8984/16/30/R03

Abstract

We review recent experiments on optical detection and manipulation of spin states of impurity centres in a solid. This research topic is of particular interest because of possible applications of the single-spin read-out technique in solid state quantum computing. The experimental background of optical detection of single quantum systems in solids is introduced. The interaction of an impurity centre with an excitation field is analysed in terms of optical Bloch equations. Recent experiments on the electron spin resonance of single organic molecules and paramagnetic defect centres in diamonds are presented. We show how the spin state of the nitrogen–vacancy paramagnetic defect in diamond can be read out optically. Pulsed electron spin resonance of the single paramagnetic defect centre in diamond is discussed.

Contents

1. Introduction 1089
2. Experimental methods 1091
3. Photophysics of a single impurity in a solid 1092
4. Magnetic resonance of the photoexcited triplet states of single organic molecules 1095
5. Optical properties of nitrogen–vacancy centres in diamond 1098
6. Optical read-out of a single spin state 1099
7. Pulsed magnetic resonance of single defect centres 1101
Conclusions and outlook 1102
Acknowledgments 1103
References 1103

1. Introduction

The growing interest in manipulation and read-out of single-electron and nuclear spin states is associated with possible applications in solid state quantum computing. The field of quantum computing has seen an explosive increase in experimental and theoretical work during the last decade. The advantage of quantum computing over classical computing lies in an exponential

speed-up of certain calculations such as Fourier transformations and searching an unordered database [1]. On the other hand, as the size of modern computer chips approaches the atomic scale, it will become necessary, in the near future, to take into account the quantum properties of individual atoms [2]. The idea of an atomic scale quantum computer is not just building atomic logic elements, but also using quantum mechanical properties for computation. Because the quantum mechanical system can exist in a superposition of several states at once, this can be used for parallel data processing. On the other hand, quantum mechanical systems are difficult to handle, and several experimental obstacles must be taken into account.

Various specific requirements on hardware for quantum computation have been identified and summarized in the Di Vincenzo check list [3]. The most successful approach for testing quantum algorithms is via liquid state NMR [4–6], which is able to realize quantum algorithms with seven qubits [7]. The main problem related to bulk NMR quantum computing is the preparation of the initial state. The density matrix of liquid state NMR is based on the initial thermal distribution of spin states. Low polarization of the initial state results in a scaling problem, which is currently one of the main obstacles to building larger scale quantum computing devices [8]. Recently, using a single nuclear spin as a qubit was proposed [9]. Note that the thermalization problem can be efficiently solved in a quantum processor, which uses single spin states for computation because reading of the spin state is equivalent to the initialization of the system. If reading of the spin state occurs on a timescale faster than the spin relaxation time, then the state is pure even for a fully thermalized spin system. However, reading a single spin state is a difficult experimental challenge. Conventional ESR and NMR spectrometers are not suitable for single-spin experiments because of the low magnetic moment associated with single electron and nuclear spins.

The typical sensitivity of inductive read-out methods is limited to 10^{16}–10^{18} spins for NMR experiments and 10^{12}–10^{14} spins for ESR. It was realized in the late 1940s that the sensitivity of magnetic resonance can be enhanced by shifting the detection of the magnetic resonance effect into the optical domain. The first experiments of this type were reported by Brossel and Bitter in 1952 [10]. The polarization of the fluorescence of mercury vapours has been monitored upon excitation of the fine structure related transition. The optical excitation produces polarization of Zeeman sublevels of the ground state of the mercury atoms. Because the Δm selection rule holds for optical transitions, the emitted radiation has circular polarization. The application of the resonance RF field equalizes populations of the fine structure sublevels, resulting in change of the fluorescence polarization. At the end of the 1960s, optically detected magnetic resonance (ODMR) had been applied to solid state systems. The rate of decay of a photoexcited triplet state of organic molecules embedded in a solid host is specific to the particular spin sublevel. Hence, the phosphorescence intensity depends on the populations of the fine structure sublevels and the application of a resonant RF field results in a change of the phosphorescence intensity. The first solid state ODMR experiments on quinoxaline were reported by Schmidt and van der Waals [11], and on phenanthrene by Sharnoff [12]. The important advantage of optical detection is the improvement of the sensitivity by seven orders of magnitude (the detection of 10^5 spins was reported in [13]). The ability to read out the state of a single nuclear spin is related to the recent achievements of single-molecule spectroscopy: an optical technique, which combines high resolution optical spectroscopy and fluorescence microscopy.

It was recognized in the early 1960s that the high absorption cross-section associated with the electronic transitions of impurities in low temperature solids can be used for ultrasensitive optical detection of aromatic compounds [14]. The detection limit for benzo[a]pyrene metabolite 50 amol was achieved for a 20 μl sample [15]. The combination of low temperature spectroscopy with high spatial resolution allowed pushing the detection limit to the ultimate frontier—single-molecule spectroscopy. The spectroscopy of single impurity molecules in low

temperature solids has been carried out in pioneering work by Moerner [16] and Orrit [17]. This was achieved by excitation of a small sample volume of pentacene-doped p-terphenyl crystal by a resonant narrow band laser. The laser-excited sample area contained thousands of dopant molecules. In order to detect individual chromophores, so-called spectral selection was applied. Individual molecules have been selected by tuning the laser frequency within the inhomogeneously broadened electronic transition of the dopant spectral site.

The transition to single-spin detection is rather obvious. Single-molecule spectroscopy can be combined with the ODMR technique in order to detect and manipulate spin states of single molecules. This spin state is a collective spin state of two unpaired electrons of the photoexcited triplet state of the organic molecule. Optical detection of such single molecular spins has been reported simultaneously by two working groups in 1993 [18, 19]. In these experiments single dopant molecules were isolated by spectral selection, and standard ODMR techniques were applied to detect spin transitions among sublevels of the photoexcited pentacene triplet state. However, the photoexcited triplet states of organic molecules are of limited interest for quantum information processing because of their short (microseconds) lifetime. The optical detection of a single paramagnetic defect in diamond opened a new perspective for single-spin based quantum computing in solids [20, 9].

2. Experimental methods

The detection of single-molecule luminescence is based on two important experimental aims. First, the concentration should be kept low enough, and the excited spot small enough, that a single impurity can be isolated in the excitation spectrum. Second, the detection efficiency must be high enough for obtaining a signal that is higher than the dark count rate of the detector.

The excited volume plays a crucial role in the experimental set-up. The signal-to-background ratio is inversely proportional to the excited volume, because all the illuminated host and guest molecules except the molecule whose fluorescence is assigned to the signal can be considered as background. A diffraction limited illuminated volume of about 1 μm^3 is achievable at room temperature, for which high numerical aperture objectives are commercially available (for a recent review see [21]). Room temperature experiments are usually based only on spatial selection of single impurities; therefore the concentration of guest molecules must be of the order of 10^{-11} M. These experiments require a simple set-up, but the low photostability of organic molecules under strong illumination is an important disadvantage for many organic systems. The photobleaching of organic molecules can be lessened by special treatment of the samples, allowing one to minimize the contact with atmospheric oxygen [22]. However, the typical lifetime of organic molecules remains below a minute. The only absolutely stable system reported so far is the vacancy–nitrogen defect centre in diamond, which will be discussed in section 5.

Tight focusing is hardly achievable at low temperatures, because the conventional optics is designed for use at ambient conditions. However, cryogenic applications open an additional possibility of selecting the guest molecules by spectral selection. This scheme is based on the phenomenon of inhomogeneous broadening of spectral lines. At cryogenic temperatures, the absorption line of the impurity is the superposition of the many sharp zero-phonon lines (ZPL [23]) of each molecule of the sample. When the number of molecules in the sample is small enough, these narrow lines can be spectrally selected by tuning the narrow band laser in resonance with the impurity centre. Low temperature spectroscopy has another advantage. At cryogenic temperature, the essential part of the oscillator strength of the absorption is concentrated in a very narrow spectral range (10^{-4} cm^{-1}). Hence, the absorption cross-

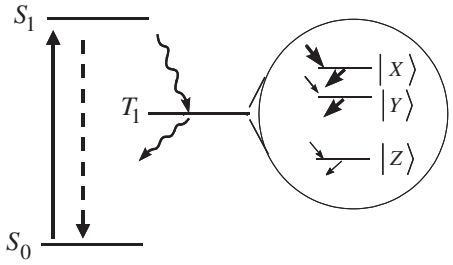

Figure 1. The energy level scheme for a single organic molecule. The inset shows the fine structure sublevels of the triplet state.

section is increased by about five orders of magnitude [24], reaching 10^{-12} cm^{-2}, which is larger than the geometric area of the impurity molecule!

The observation of narrow zero-phonon lines is, however, restricted to a relatively limited number of host–guest systems, which shows the Spolskii effect. The origin of the Spolskii effect has been discussed in the literature (for recent work see [25–27]). To present a strong and stable ZPL, the impurity molecule must fit into an insertion site of the matrix, and its vibrational frequency, associated with local matrix vibration, must be as high as possible. This situation occurs when the size of the guest molecule corresponds to the size of the vacancy created by one or a few impurity molecules absent from the lattice [28].

The presence of spectrally stable and sharp zero-phonon lines is not sufficient for successful detection of a single molecule. The dopant molecules are detected via fluorescence emission. Hence, the optical transition must carry strong oscillator strength and only allowed singlet–singlet (or triplet–triplet) transitions can be considered. The study of single-molecule fluorescence requires consecutive detections of at least several thousand photons. Hence the host and guest molecules must be photochemically stable.

3. Photophysics of a single impurity in a solid

The spectroscopy of single impurities isolated in a matrix has made important progress during the last decade and become the standard technique in a number of research laboratories. Although the first single-molecule experiment, reported by Moerner [16], was based on absorption spectroscopy, all modern approaches are based on the detection of the fluorescence emission because of the superior signal-to-noise ratio (this technique was introduced by Orrit [17]). The optical transition associated with the impurity molecule must be strong enough to produce a detectable fluorescence signal. Electronic transitions of an organic impurity can be approximated by a three-level system, including ground S_0 and excited S_1 singlet electronic states and the photoexcited triplet state T_1 (see figure 1). In a typical experiment, the molecule is illuminated with laser light in resonance with the $S_0 \rightarrow S_1$ transition and Stokes-shifted fluorescence emission is detected. After being excited in the S_1 state the molecule can either relax back to the ground state via fluorescence emission and internal conversion, or can be trapped in the triplet state via the intersystem crossing process. In the inset of the figure 1, the sublevels of the triplet state related to zero-field splitting are shown.

The dynamics of a molecule under coherent optical excitation can be described in terms of optical Bloch equations describing a pseudospin which performs Rabi oscillations between the ground and excited electronic states [29]. In the rotating wave approximation the evolution

of the density vector for a three-level system is described by [29]

$$\begin{aligned}
\dot{\sigma}_{11} &= k_{21}\sigma_{22} + k_{31}\sigma_{33} + \frac{\mathrm{i}\Omega}{2}(\sigma_{21} - \sigma_{12}),\\
\dot{\sigma}_{22} &= -(k_{21} + k_{23})\sigma_{22} + \frac{\mathrm{i}\Omega}{2}(\sigma_{12} - \sigma_{21}),\\
\dot{\sigma}_{33} &= k_{23}\sigma_{22} - k_{31}\sigma_{33},\\
\dot{\sigma}_{12} &= -\frac{\mathrm{i}\Omega}{2}\sigma_{11} + \frac{\mathrm{i}\Omega}{2}\sigma_{22} + (\mathrm{i}\Delta - \Gamma_2)\sigma_{12},
\end{aligned} \tag{1}$$

where a normalization condition for the populations holds: $\sigma_{11} + \sigma_{22} + \sigma_{33} = 1$. $\Gamma_2 = \frac{1}{T_2} = \frac{1}{2T_1} + \frac{1}{T_2^*}$ is the dephasing rate of the $S_0 \rightarrow S_1$ transition, T_1 and is the relaxation time, T_2^* is the pure dephasing time of the optical transition, Δ is the detuning of the excitation field from the frequency of the $S_0 \rightarrow S_1$ transition, k_{ij} are incoherent transition rates. Ω is the Rabi frequency of the resonant optical field: $\Omega = \frac{|\vec{\mu}\vec{E}|}{\hbar}$, where $\vec{\mu}$ is the transition dipole moment and $\vec{E}$ is the optical field. Here, level 3 is the metastable triplet level.

The Bloch equations can be solved analytically. The steady state solution $\dot{\sigma}_{11} = \dot{\sigma}_{22} = \dot{\sigma}_{33} = 0$ of the Bloch equations gives access to the steady state population of the excited state and the linewidth of the spectral line, corresponding to the $S_0 \rightarrow S_1$ transition. As was shown in [30], the linewidth and fluorescence emission rate of the molecule can be expressed as follows:

$$\Delta\nu(I) = \Delta\nu(0)\sqrt{1 + I/I_S}, \tag{2}$$

$$R(I) = \sigma_{22}\frac{1}{\tau_{Fl}}\phi_{Fl} = R_\infty\frac{I/I_S}{1 + I/I_S}. \tag{3}$$

Here I is the excitation intensity, τ_{Fl} is the fluorescence lifetime, $\tau_{Fl} = 1/(k_{21} + k_{23})$, I_S is the saturation parameter, which can be expressed as

$$I_S = \frac{\varepsilon_0 c\hbar\left(k_{21} + \sum_i k_{23}^i\right)}{|\vec{\mu}|^2(2 + A)T_2}, \tag{4}$$

where $A = \sum_i k_{23}^i/k_{31}^i$, k_{23}^i and k_{31}^i are the intersystem crossing rates corresponding to the transitions to and from different fine structure sublevels of the photoexcited triplet state. Equations (3) and (4) can be combined to give the saturated emission rate:

$$R_\infty = \frac{\phi_{Fl}\left(k_{21} + \sum_i k_{23}^i\right)}{2 + A}. \tag{5}$$

The maximum emission rate of such a system is determined by the fluorescence quantum yield, but also by the rate of trapping to the metastable triplet state and by the rate of depopulation of this state. Hence the triplet state parameters play a crucial role in the choice of the system for single-molecule spectroscopy. For dibenzanthanthrene in a naphthalene matrix, $k_{23}^{x,y}$, k_{23}^z, $k_{31}^{x,y}$, k_{31}^z are 480, 5400, 30, 900 s^{-1}, respectively [31, 32]. The contribution of the triplet to saturation is small and the fully saturated signal is reduced by about 8% with respect to that of a pure two-level system. Note that the long living metastable state seriously affects the saturated signal even if the fluorescence quantum yield is high.

Figure 2 shows an experimental study of the linewidth of a single-molecule spectral line as a function of the excitation intensity. The results are in very good agreement with the expected power broadening law. The fit gave homogeneous widths of 25 MHz, with errors of a few megahertz. The inset to figure 2 shows an example of a single-molecule excitation line at weak and strong exciting intensity. The line is roughly Lorentzian and shows power broadening when the laser power is high.

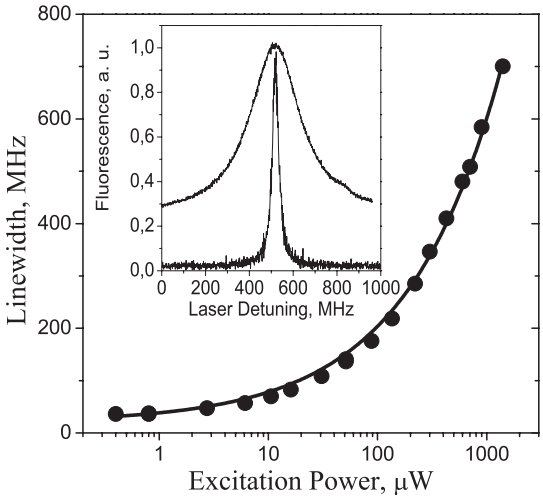

Figure 2. The excitation power dependence of the excitation linewidth of a single dibenzoterrylene molecule in a naphthalene host at $T = 1.6$ K. The inset shows the fluorescence excitation lines recorded at high and low laser lower.

The time distribution of photons emitted by a single molecule gives access to its internal photophysical processes. In order to describe the inhomogeneity of photons emitted by a single molecule, it is useful to introduce the second-order autocorrelation function $g^{(2)}(\tau)$, defined as follows:

$$g^{(2)}(\tau) = \langle I(t)I(t+\tau)\rangle / \langle I(t)\rangle^2, \tag{6}$$

where

$$\langle I(t)I(t+\tau)\rangle = \lim_{T\to\infty} \frac{1}{T}\int_0^T I(t)I(t+\tau)\,\mathrm{d}t.$$

Here, $I(t)$ is the fluorescence intensity emitted by a single molecule at time t. As was shown by Orrit and co-workers, the autocorrelation function can be deduced from the measurements of photocount pairs separated by a given time interval [33]. The probability of detecting a pair of photons separated by an interval τ is proportional to the probability of finding the molecule in an excited state at time t and the probability that the molecule will be in the excited state at time $t+\tau$. There is also a connection between the autocorrelation function and the time dependent solution of the Bloch equations. The probability of finding the molecule in the excited state is proportional to the matrix element σ_{22}. The transient solution of the Bloch equation can be found by applying the Laplace transform technique. The solution for the correlation function with the triplet state contribution neglected can be expressed as follows:

$$g^{(2)}(\tau) = 1 - \exp\left(-\frac{(\Gamma_2 + k_{21})\tau}{2}\right)\left(\frac{(\Gamma_2 + k_{21})}{2\Omega}\sin(\Omega\tau) + \cos(\Omega\tau)\right). \tag{7}$$

Here, Γ_2 is the dephasing rate of optical transition of the optical transition and k_{21} is the radiative decay rate of the excited state. Figure 3 shows the results of a measurement of the correlation function for a single dibenzanthanthrene molecule isolated in a naphthalene host. There are several remarkable features visible from the correlation function. The zero-time value of the autocorrelation function tends to zero. Note that for the coherent light field, the zero-time value of $g^{(2)}$ is unity [34]. The value of the correlation function below unity indicates the non-classical nature of the fluorescence emitted by a single molecule. The emission of

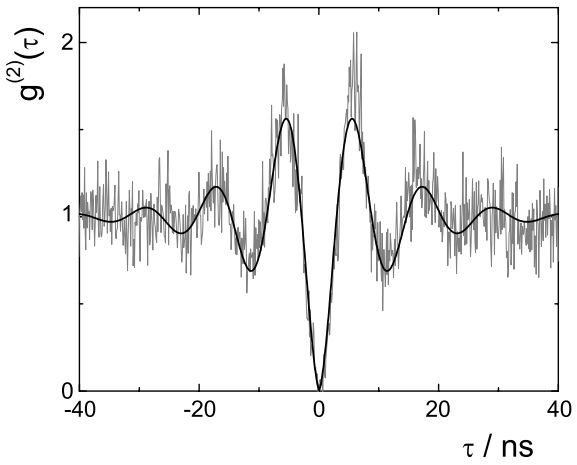

Figure 3. The fluorescence intensity autocorrelation function for a single dibenzanthanthrene molecule isolated in a naphthalene host. The fit function follows equation (7).

photons by a single quantum system can be characterized by the so-called antibunching effect. The antibunching effect is related to projection type measurements, performed on a single quantum system. The observation of the first photon projects the system into the ground state. In order to emit the second photon the system must be excited again. The probability of emitting the second photon at time zero is zero because the system cannot emit a photon from the ground state. The situation will be different for a larger number of molecules. For an ensemble consisting of several molecules, there is a probability of obtaining a situation where more than two emitters are in the excited state. Therefore, there is a finite probability of simultaneous emission of photons and thus $g^{(2)}(0) > 0$. In general, the contrast is decreased by a factor of N, where N is the number of molecules.

It also can be seen from the figure 3 that the value of the correlation function increases to a higher value, showing damped oscillations. The Rabi oscillations correspond to the coherent evolution of resonantly driven two-level systems. The decay of the oscillations is related to a dephasing process, which occurs in the singlet excited state. The dephasing rate is mostly determined by the radiative decay in the temperature range between 1 and 10 K. At higher temperatures, the damping is stronger, because the pure dephasing processes related to electron–phonon interactions become active.

4. Magnetic resonance of the photoexcited triplet states of single organic molecules

Under continuous optical excitation, the average fluorescence emission is determined by the population and depopulation rates of the triplet state sublevels (see equation (5) and figure 1). For the case of organic molecules the rates for the three sublevels differ significantly. This is the result of the high selectivity of the intersystem crossing process, which is related to the fact that the spin–orbit coupling can mix the singlet character only into specific triplet sublevels. Usually, the $|X\rangle$ and $|Y\rangle$ sublevels have a much higher probability of population than $|Z\rangle$. These two levels also have much shorter lifetimes. This creates a considerable population difference between the three triplet sublevels. Irradiation with microwaves resonant with either the $|X\rangle$–$|Z\rangle$ or $|Y\rangle$–$|Z\rangle$ transition leads to a redistribution of the population of the two levels involved in the resonance and hence to a change of the average lifetime of the triplet

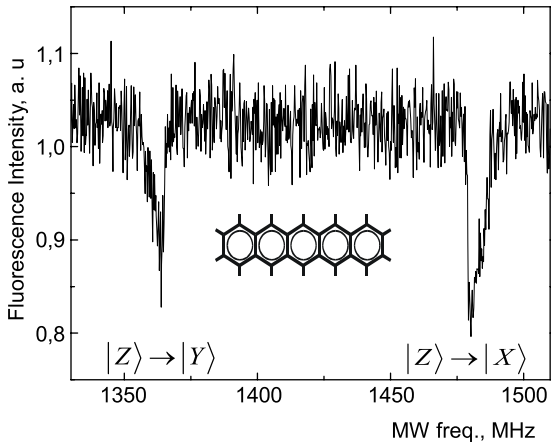

Figure 4. The ODMR spectrum of a single pentacene molecule. The inset shows the chemical structure of pentacene.

state. This in turn affects the population of the ground state and, since the system is excited continuously, leads to a change of the fluorescence intensity.

The Hamilton operator of the triplet system without a nuclear Zeeman terms is

$$H = \vec{S} \cdot \overleftrightarrow{D} \cdot \vec{S} + \beta_e g_e \vec{S} \cdot \vec{B}_0 + \sum_i \vec{S} \cdot \overleftrightarrow{A}^{(i)} \vec{I}_i, \tag{8}$$

where $\vec{S}$ is the electron spin operator ($S = 1$), $\vec{I}_i$ is the nuclear spin operator of the nucleus i, $\overleftrightarrow{D}$ is a fine structure tensor, β_e is the Bohr magneton of the electron, g_e is the electron g-value, $\vec{B}_0$ is the external magnetic field, $\overleftrightarrow{A}^{(i)}$ is the hyperfine interaction tensor of nucleus i. The hyperfine interaction term includes all nuclei, intramolecular and intermolecular, coupled to the electron spin.

The first term in the spin Hamiltonian, $\vec{S} \cdot \overleftrightarrow{D} \cdot \vec{S}$, leads to a zero-field splitting of the triplet state sublevels as a result of the (magnetic) dipole–dipole interaction of the two unpaired electron spins. The second term, $\beta_e g_e \vec{S} \cdot \vec{B}_0$, corresponds to the interaction of the electron spin with an externally applied magnetic field. The third part of the spin Hamiltonian describes the interaction of the electron spin with the surrounding nuclear spins.

The conventional ODMR technique can be applied in single-molecule studies when optical selection of single molecules is possible [35–37, 19]. Figure 4 shows the ODMR spectrum of a single pentacene molecule isolated in a para-terphenyl host at $T = 1.6$ K. The laser was tuned to the peak of the single-molecule fluorescence excitation line and the power was adjusted to saturate the optical $^1S_1 \leftarrow {}^1S_0$ transition. The fluorescence intensity was monitored as a function of the microwave frequency. The spectrum shows that, even in zero magnetic field, the triplet state of pentacene is split into the three zero-field eigenstates $|X\rangle$, $|Y\rangle$ and $|Z\rangle$. In figure 4 the $|Y\rangle$–$|Z\rangle$ and the $|X\rangle$–$|Z\rangle$ magnetic resonance transitions are observed as a decrease (up to 25%) of the fluorescence. This is caused by the increased population probability of the long lived $|Z\rangle$ level. The third transition ($|X\rangle$–$|Y\rangle$) is much weaker due to unfavourable population and depopulation kinetics.

Note that the single-molecule ODMR lines show an asymmetric lineshape with a steep decrease towards higher microwave frequencies for both the single-molecule and the ensemble case. The lineshape results from the hyperfine interaction of the triplet electron spin with the pentacene proton spins ($I = 1/2$). Each proton can exist in one of its two nuclear spin states,

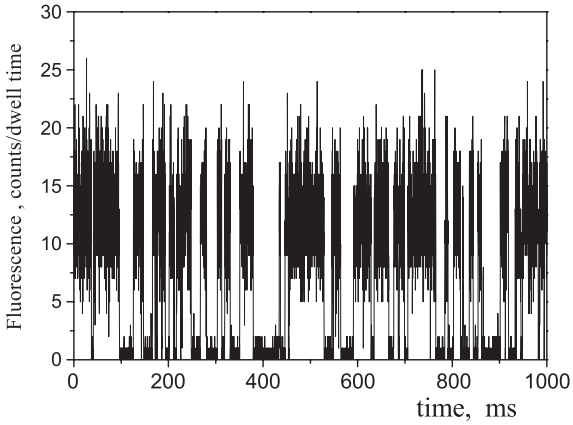

Figure 5. The fluorescence signal from a single terrylene molecule.

which yields 2^{14} nuclear spin configurations. The hyperfine interaction of each of these nuclear configurations causes a slight shift of the resonance. For a single molecule one would expect it to 'see' only one nuclear spin configuration and a very narrow magnetic resonance line to be observable. Apparently, the molecule experiences all of these configurations during the many optical pumping cycles which are needed to accumulate a sufficient signal-to-noise ratio. This is due to the dipolar coupling among the proton spins, which leads to a spin diffusion within the proton reservoir of the guest and the host. When the triplet magnetic moment is created, the 14 protons spins on the pentacene suddenly 'feel' the (second-order) hyperfine fields, which shift their resonance frequency away from the dipolar spectrum of the protons in the bulk of the crystal. Consequently, during the triplet lifetime, this configuration is frozen and the resonance frequency can only vary in a small interval $\Delta\nu$ determined by the flip-flop motions of the protons in the bulk. This interval can be estimated from the electron spin–spin relaxation time T_2 and amounts to $\Delta\nu = \frac{1}{\pi T_2} \approx 150\,\mathrm{kHz}$ [38, 37]. On return to the ground state, the hyperfine fields disappear and the pentacene protons are free to participate in the nuclear flip-flop motion. When the molecule is excited again into the triplet state, a new magnetic configuration is frozen, which corresponds to a different position of the zero-field resonance line. An estimate of the related timescales yields that the average time between two excitations into the triplet state is about 20 μs and that the mean residence time of the molecule in the triplet state is about 50 μs. For the inverse of the flip-flop rate one can estimate a value of about 30 μs which means that each time the molecule reappears in the triplet state it experiences a different nuclear configuration. Since some hundred thousand cycles are averaged for the spectrum in figure 4 the same linewidth is found as in ensemble experiments.

Single-molecule spectroscopy is performed by detection of fluorescence originating from strongly driven singlet–singlet transitions. This excitation–emission cycle is repeated millions of times per second in order to produce a high enough signal. Occasionally, if the single molecule is trapped in the metastable triplet state, the stream of emitted photons becomes interrupted. The fluorescence emission time trace of a single pentacene molecule is shown in figure 5. The length of the corresponding dark time interval of fluorescence emission is determined by the lifetime of the triplet state. Because the different triplet sublevels have different decay rates, the histogram of the dark time is determined by contributions of different triplet state sublevels. It was demonstrated that microwave-induced changes of the distribution of the dark intervals could be used to detect transitions between triplet sublevels.

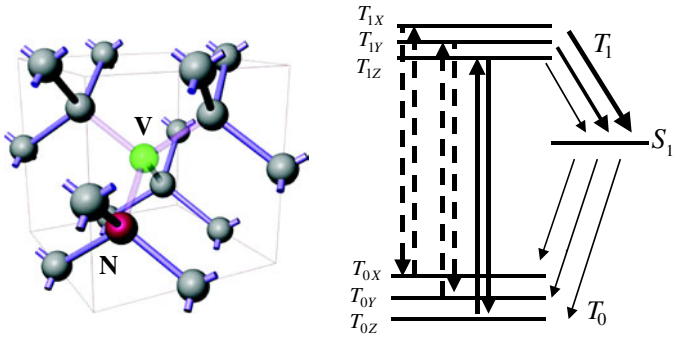

Figure 6. The model of the structure (left) and the energy level scheme (right) for the nitrogen–vacancy centre in diamond.

By synchronizing resonant microwave pulses with the quantum jumps of a terrylene molecule, the high contrast transient ODMR signal was detected [39].

Although a number of classical experiments have been performed on the photoexcited triplet states of single molecules, including transient nutations, Hahn echo and electron–nuclear double-resonance (ENDOR) studies [40–42, 19, 37], these systems always require a time averaged read-out. When a photodetector records no counts, which corresponds to the beginning of the dark interval (see figure 5), it is impossible to determine in which sublevel of the triplet state the molecule is trapped. In order to obtain this information, it is necessary to know the duration of the dark interval and one needs to wait a while before the next photon burst is detected. But at this time, the molecule is no longer in the triplet state. Therefore, the measurement of the spin state always takes longer than the T_1 time of the spin state. On the other hand, quantum computing requires read-out schemes which are able to determine the spin state within the T_1 time. This was demonstrated for the nitrogen–vacancy defect centre in diamond, which is a system with a paramagnetic ground state.

5. Optical properties of nitrogen–vacancy centres in diamond

Although a large number of paramagnetic and optically active defects centres in solids are known, most of them cannot be detected as single centres because they show very weak oscillator strength and/or the presence of metastable states, which limits the magnitude of the fluorescence signal. The nitrogen–vacancy (N–V) defect has, up to now, been the only paramagnetic system which can be detected optically as a single centre. The N–V defect is a naturally occurring defect in diamond with nitrogen impurities. This defect centre is particularly intense in type Ib synthetic diamond (diamonds with isolated substitutional nitrogen contents of about 100 ppm). In those diamonds, N–V defects can be produced by irradiation and subsequent annealing at temperatures above 550 °C. Radiation damage creates vacancies in the diamond lattice. Annealing treatment leads to migration of vacancies towards nitrogen atoms creating N–V defects. The N–V centre can also be produced in type IIa diamonds (low nitrogen content diamonds containing less than 20 ppm of nitrogen) by N^+ ion implantation. The centre shows a linear Stark effect, which is due to the absence of inversion symmetry. Figure 6 shows the generally accepted model of the N–V centre. On the basis of neutron irradiation experiments, Mita and co-workers have reported that the N–V centre is negatively charged [43].

The fluorescence spectrum of the centre consists of a sharp zero-phonon line at 638 nm (1.945 eV) [44, 45]. In ^{13}C diamonds the zero-phonon line of the centre is blue-shifted by 2.1 meV [46]. The oscillator strength of the optical transition of the N–V centre is comparable with that of the GRI centre (the neutral vacancy in diamond). The fluorescence quantum yield is 0.99 [47]. The electron–phonon coupling is strong (the Huang–Rhys factor $S = 3.65$) and dominated by coupling to 65 meV phonon modes. The fluorescence lifetime of the centre is 11.6 and 13.3 ns at 77 and 700 K respectively [48, 47].

The energy level scheme of the N–V centre is shown in figure 6. It consists of a triplet ground state (T_0) and a triplet excited state (T_1). The scheme also includes a transition to the metastable singlet state (S_1). At zero magnetic field, the ground triplet state of the centre is split by the coupling of two unpaired electron spins in the diamond crystal field into three sublevels X, Y ($m_S = \pm 1$) and Z ($m_S = 0$), separated by 2.88 GHz [49, 50]. The excited state has a more complicated fine structure, originating from spin–spin and spin–orbit interactions and from strain in the crystal. It consists of two groups, each with three sublevels separated by a few GHz within each group. The energy separation between the groups is about 40 wavenumbers [51]. The substates show a fast decay to the lower lying excited state level [52–54, 49]. Only the lowest three spin sublevels of the excited triplet state are shown here.

6. Optical read-out of a single spin state

The splitting between sublevels of two triplet states is larger than the homogeneous linewidth of the optical transition at $T = 2$ K. Hence, site selective excitation can be used as a tool to determine the state of the defect centre spin. When the narrow band laser is tuned in resonance with the transition between a specific pair of spin sublevels T_{0i} and T_{1j}, the defect centre can be excited to the T_1 state. Here we assume that the sublevel T_{0i} has nonzero initial population and that the transition $T_{0i} \rightarrow T_{1j}$ is allowed by the selection rules. The probability of transition is proportional to $|\langle S_i|S_j\rangle|^2$, where the S_i and S_j are the spin wavefunctions of the T_{0i} and T_{1j} substates. In general, the principal spin axes X, Y, Z of the ground triplet state may be different from those of the excited triplet level due to different distributions of the electronic density of the two unpaired electrons. Hence, it can be anticipated that electronic transitions from every spin sublevel of the ground state to every spin sublevel of the excited state are possible. On the other hand, the symmetry of a defect often give an invariant direction of the principal spin axes [55]. Therefore, taking into account the C_{3v} symmetry of the N–V defect, the conservation of principal spin axes can be assumed. In this case, the only allowed electronic transitions are those between sublevels of the same spin components: $T_{0i}T_{1i}$. Thus, there are three optically allowed transitions, which are shown in figure 6 by pairs (for excitation and emission) of vertical lines. Due to different zero-field splittings in the ground and excited states [51], those three optical resonances will appear at different spectral positions when the laser is scanned through the T_0–T_1 absorption band and three peaks can be expected in the fluorescence excitation spectra.

The fluorescence excitation spectrum of a single N–V centre is shown on figure 7. Surprisingly only a single excitation line appears in the excitation spectrum. The single-centre absorption line has a Lorentzian shape. The linewidth of around 280 MHz is larger than the limit imposed by radiative decay of the excited triplet state. The line broadening can be attributed to spectral diffusion processes. Since the spectral width of a single centre is much narrower than the zero-field splitting in the ground state $\Delta E = 2.88$ GHz, the excitation line shown in figure 7 marks a specific spin configuration of the defect. The absence of satellites related to transitions between other sublevels has been explained by sublevel-specific intersystem crossing parameters [56]. When the excitation laser is in resonance with the T_0–T_1

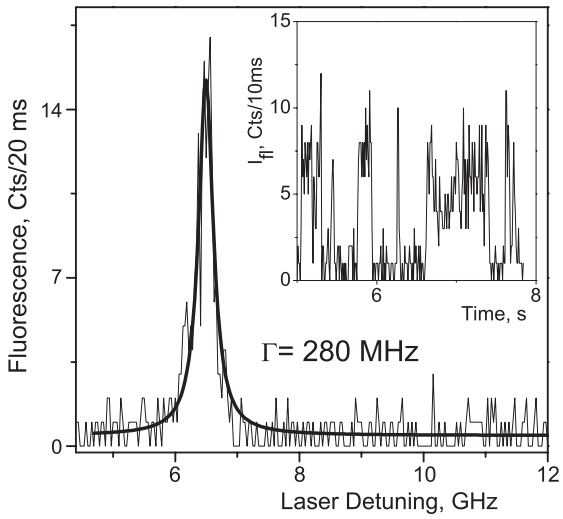

Figure 7. The fluorescence excitation line of the N–V centre in diamond at $T = 1.6$ K. The fit curve is a Lorentzian function. The inset shows the time trace of the fluorescence signal when the excitation laser was tuned to the resonance of the transition.

transition, the fluorescence exhibits a telegraph behaviour. This is shown in figure 7, where the fluorescence of a single N–V defect is plotted as a function of time. The duration of bright intervals decreases upon increase of the excitation intensity, indicating a photoinduced process.

A detailed analysis of the excitation–emission pathway is necessary for explanation of blinking behaviour. There are three different excitation pathways for a single defect centre. First, as long as an optically excited defect centre remains in one of the T_{1i}–T_{0i} channels, it emits fluorescence. The emission rate is rather high, typically of the order of tens of megahertz. Second, the defect centre can also undergo intersystem crossing from T_{1i} to the singlet state S, which is characterized by the rate $k_{i\mathrm{S}}$ specific to this T_{1i} sublevel. As soon as an intersystem crossing to S takes place, the single-defect-centre transition becomes out of resonance with the driving laser field, and no fluorescence is expected to occur. Third, the defect centre can return to the ground triplet T_0 within the lifetime of the metastable singlet state, which is typically much longer than the radiative lifetime of the excited triplet state. Within this picture, there are three possibilities for this transition, differing in the final substate of the ground triplet state T_0. Only one of them, the ISC transition $\mathrm{S} \rightarrow T_{0i}$, brings the molecule back into resonance with the excitation laser, thus resulting in the termination of the dark interval in the fluorescence and restoration of fluorescence emission. Note that the complete pathway $T_{1i} \rightarrow \mathrm{S} \rightarrow T_{0i}$ conserves spin projection.

The other intersystem crossing transitions, involving a change in spin projection, do not return the molecule into resonance with the laser because of the large zero-field splitting in the ground triplet state. To restore fluorescence in this case, a spin relaxation transition must take place. This thermally activated process is known to be slow (of the order of seconds) at liquid helium temperatures. Another mechanism is the coupling of the triplet electronic spin of the single impurity studied in the T_0 state to electronic spins T_0 of other defects of the same type in a host lattice. These spin–spin interactions result in flip-flop processes between different centres (cross-relaxation), nearly equalizing the T_0 substate populations of the optically excited centre. However, the latter mechanism is effective only at large concentrations of defect centres, while experiments with single centres are performed on samples with a low N–V centre concentration.

If some of the pathways $T_{1i} \rightarrow S \rightarrow T_{0n}$ ($n \neq i$) become more active, this will increase the durations of dark periods in the fluorescence.

The appearance of a single line in the excitation spectrum can be understood as follows. Let us consider in more detail the case where the laser is tuned in resonance with the fine structure transition between the T_{0Z} and T_{1Z} substates, as shown in figure 6 with solid vertical lines. In this case the system can be described in terms of the general optical Bloch equations. The average fluorescence intensity emitted by a single molecule can be written as [56]

$$I_{FL} = \frac{AB}{3(A + B + k_S) + B\left(1 + \frac{k_S}{R}\frac{k_X + k_Y + R}{k_Z}\right)}, \tag{9}$$

where A and B are the rates of spontaneous emission and absorption corresponding to the transition $T_{1Z} \rightarrow T_{0Z}$. k_S is the singlet population rate corresponding to the transition $T_{1Z} \rightarrow S$. k_X, k_Y and k_Z are the singlet rates of depopulation toward ground state sublevels X, Y and Z, respectively. R is spin–lattice relaxation rate. If R is much lower than the rate of decay of the excited singlet state, the fluorescence signal under complete optical saturation can be written as $I_{FL}^{\infty} = \frac{AR}{k_S}$. By substituting here the expected rates $R \sim 1\ s^{-1}$, and $A \sim 10^8\ s^{-1}$ and $k_S \sim 10^3\ s^{-1}$, and taking into account the detection efficiency of the set-up $\sim$1%, the fluorescence signal can be estimated to be of the order of a few thousand photocounts per second, which is in good agreement with the experimental data. Note that faster shelving rates have been recently observed from correlation measurements on single N–V centres [57–59]. These are attributed to the k_S for the other transitions. If one of those other transitions is pumped, i.e. $T_{0X;Y} \rightarrow T_{1X;Y}$, then the intersystem crossing rate k_S is three orders of magnitude larger ($k_S \sim 10^6\ s^{-1}$) and a rate of roughly 0.1–1 detectable photocounts per second is calculated. The intersystem crossing rate is thus essential for the possibility of detecting the resonance lines of individual defects. Spectral hole burning experiments show $k_S = 12.4$ kHz, which can be attributed to shelving from the Z sublevel [60]. The intersystem crossing process for X and Y sublevels of the triplet excited state is probably faster. The conclusion is that those resonant lines corresponding to sublevels other than the $T_{1Z} \rightarrow T_{0Z}$ are not observable because of the low fluorescence intensity, according to equation (9).

7. Pulsed magnetic resonance of single defect centres

The manipulation of single spin states is of great importance for quantum computing applications. Single-spin coherence in solids has been observed for organic systems [39, 37]. However, coherent experiments on the N–V centre are of particular interest for two reasons. First, the spin coherence time is not limited by the electronic lifetime of the excited triplet state. Second, as was discussed above, the spin state of the N–V centre can be detected directly via optical excitation.

The simplest coherence spin resonance experiment is the detection of transient nutations. In this experiment a resonant microwave field is applied to the sample. This microwave field induces transitions between ground state sublevels, resulting in a spin precession in the direction perpendicular to the direction of the applied field in the rotating frame. This is equivalent to a periodic change of population of the spin sublevels.

Several experimental aspects related to measurements on a single spin must be pointed out. First, the measurement of a single spin is projective, i.e. read-out always projects the spin state into one of the eigenstates. Therefore, coherent experiments require several measurements for detection of coherent oscillations. Second, it is necessary to initialize the state of the spin at the beginning of the experiment. This can be achieved by a strong non-selective excitation, which drives the N–V centre into the Z sublevel of the triplet ground state. Third, the projective

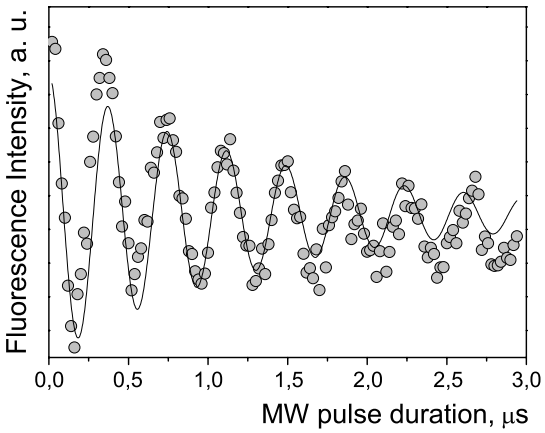

Figure 8. Transient nutations of the electron spin between ground state sublevels of a single N–V defect. The spin state has been initialized by a non-selective optical pulse. Subsequently, a resonant microwave pulse of variable duration was applied. The state was read out optically. 10^6 measurements were accumulated to obtain a smooth curve. The fit curve represents an exponentially decaying harmonic function.

nature of the spin detection leads to the feature that a continuous measurement of the spin state induces decoherence [61].

Figure 8 shows a transient nutation experiment on a single N–V centre. The system was polarized into the $m_S = 0$ sublevel by a strong unselective illumination. After that, the laser was switched off and a microwave pulse of variable duration was applied. The read-out of the spin state was achieved by monitoring the fluorescence intensity. The experimental data clearly demonstrate a periodic modulation of the fluorescence signal. This corresponds to coherent oscillation of the electronic spin between the $m_S = 0$ and 1 sublevels. The fluorescence intensity starts at a high level, corresponding to population of the $m_S = 0$ sublevel. Upon increasing the pulse length, the fluorescence intensity decreases, reaching the case of population inversion at a pulse duration of 160 ns (π-pulse). Note that the coherent nutation experiment is equivalent to realization of a NOT gate, which is essential for quantum computation schemes.

The decay of coherent oscillations is determined by the electron spin dephasing time T_2, which typically ranges from 1.5 to 3 μs, depending on the defect centre under study. Recently, ensemble experiments have shown that T_2 in this system can reach values larger than 60 μs, with increasing T_2 in samples with low nitrogen content [62]. The most important dephasing mechanism is spin flip-flop processes, either directly between electron spins of the N–V centre and residual nitrogen impurities in the diamond lattices (P centre, $S = 1/2$) or via hyperfine coupling to the nitrogen nuclear spin. In both cases, the dephasing rate is strongly distance dependent ($1/r^3$). The differences among the T_2 values of different N–V centres are possibly due to a change in the distance between the electron spin of the centre and the nearest neighbour nitrogen in the lattice.

Conclusions and outlook

The accurate measurement of a single spin state has two important aspects. First, single-spin magnetic resonance is a central point for any pure state based quantum computing scheme. Several promising techniques are currently under investigation. Recently, controlled electron spin injection and single-spin detection were demonstrated using electrical read-out in quantum

dots [63, 64] and scanning tunnelling microscopy of organic molecules [65]. Important progress has been achieved in the field of magnetic resonance force microscopy [66, 67], which recently showed detection sensitivity of two electron spins [68]. Yet optical detection remains a unique technique, capable of demonstrating coherent ESR and NMR in experiments on single quantum systems [69]. The next step will be to show coupling between several spins. This will allow achievement of two-qubit gates, which are basic elements for quantum computing.

The second important field is of more fundamental character. Experiments with single spins are suitable for experimental testing of quantum mechanics. Projective spin measurements on single quantum systems can be used in tests of the quantum Zeno effect and Bell's inequalities.

Acknowledgments

We acknowledge financial support of our research projects by DFG (programme 'Quanten-Informationsverarbeitung'), Landesstiftung BW and EU (IST project 'QIPDDF-ROSES'). Some of the experimental results presented here were obtained by Achim Gruber, Iulian Popa and Torsten Gaebel. We thank Iulian Popa for a critical reading of the manuscript. Experimental data presented figures 2 and 4 have been obtained at CPMOH (University of Bordeaux) and OSMP (University of Chemnitz), respectively.

References

[1] Shor P W 2003 *J. ACM* **50** 87
[2] Datta S 1997 *Electronic Transport in Mesoscopic Systems* (Cambridge: Cambridge University Press)
[3] Divincenzo D P 1995 *Science* **270** 255
[4] Gershenfeld N A and Chuang I L 1997 *Science* **275** 350
[5] Gershenfeld N and Chuang I L 1998 *Sci. Am.* **278** 66
[6] Brassard G, Chuang I, Lloyd S and Monroe C 1998 *Proc. Natl Acad. Sci. USA* **95** 11032
[7] Vandersypen L M K, Steffen M, Breyta G, Yannoni C S, Sherwood M H and Chuang I L 2001 *Nature* **414** 883
[8] Warren W S 1997 *Science* **277** 1688
[9] Wrachtrup J, Kilin S Y and Nizovtsev A P 2001 *Opt. Spectrosc.* **91** 429
[10] Brossel J and Bitter F 1952 *Phys. Rev.* **86** 308
[11] Schmidt J and van der Waals J H 1968 *Chem. Phys. Lett.* **2** 640
[12] Sharnoff R 1967 *J. Chem. Phys.* **46** 3262
[13] Clarke R H 1982 *Triplet State ODMR Spectroscopy* (New York: Wiley)
[14] Personov R I 2003 *Zh. Anal. Khim.* **17** 506
[15] Weeks S J, Gilles S M and Dsilva A P 1991 *Appl. Spectrosc.* **45** 1093
[16] Moerner W E and Kador L 1989 *Phys. Rev. Lett.* **62** 2535
[17] Orrit M and Bernard J 1990 *Phys. Rev. Lett.* **65** 2716
[18] Kohler J, Dosselhorst J A J M, Donckers M C J M, Groenen E J J, Schmidt J and Moerner W E 1993 *Nature* **363** 242
[19] Wrachtrup J, von Borczyskowski C, Bernard J, Orrit M and Brown R 1993 *Nature* **363** 244
[20] Gruber A, Drabenstedt A, Tietz C, Fleury L, Wrachtrup J and von Borczyskowski C 1997 *Science* **276** 2012
[21] Moerner W E and Fromm D P 2003 *Rev. Sci. Instrum.* **74** 3597
[22] English D S, Furube A and Barbara P F 2000 *Chem. Phys. Lett.* **324** 15
[23] Rebane K K 2002 *J. Lumin.* **100** 219
[24] Rebane K K and Rebane I 1993 *J. Lumin.* **56** 39
[25] Matsushita M, Bloess A, Durand Y, Butter J Y P, Schmidt J and Groenen E J J 2002 *J. Chem. Phys.* **117** 3383
[26] Bloess A, Durand Y, Matsushita M, Schmidt J and Groenen E J J 2001 *Chem. Phys. Lett.* **344** 55
[27] Bloess A, Durand Y, Matsushita M, Verberk R, Groenen E J J and Schmidt J 2001 *J. Phys. Chem.* A **105** 3016
[28] Shpolski E V 1962 *Usp. Fiz. Nauk* **77** 321
[29] Bernard J, Fleury L, Talon H and Orrit M 1993 *J. Chem. Phys.* **98** 850
[30] Ambrose W P, Bashe T and Morner W E 1991 *J. Chem. Phys.* **95** 7150

[31] Jelezko F, Lounis B and Orrit M 1997 *J. Chem. Phys.* **107** 1692
[32] Lounis B, Jelezko F and Orrit M 1997 *Phys. Rev. Lett.* **78** 3673
[33] Brown R, Wrachtrup J, Orrit M, Bernard J and von Borczyskowski C 1994 *J. Chem. Phys.* **100** 7182
[34] Loudon R 1983 *The Quantum Theory of Light* (Oxford: Oxford University Press)
[35] Vogel A, Gruber A, Wrachtrup J and von Borczyskowski C 1995 *J. Phys. Chem.* **99** 14915
[36] Silbey R J 1993 *Nature* **363** 214
[37] Wrachtrup J, von Borczyskowski C, Bernard J, Orrit M and Brown R 1993 *Phys. Rev. Lett.* **71** 3565
[38] van Strien A J and Schmidt J 1980 *Chem. Phys. Lett.* **70** 513
[39] Brouwer A C J, Groenen E J J and Schmidt J 1998 *Phys. Rev. Lett.* **80** 3944
[40] Köhler J, Disselhorst J A J M, Donckers M C J M, Groenen E J J, Schmidt J and Moerner W E 1993 *Nature* **363** 242
[41] Köhler J, Brouwer A C J, Groenen E J J and Schmidt J 1994 *Chem. Phys. Lett.* **228** 47
[42] Köhler J, Brouwer A C J, Groenen E J J and Schmidt J 1995 *Science* **268** 1457
[43] Mita Y 1996 *Phys. Rev.* B **53** 11360
[44] Davies G 1994 *Properties and Growth of Diamond* (London: INSPEC)
[45] Davies G and Hamer M F 1976 *Proc. R. Soc.* A **384** 285
[46] Collins A T, Davies G, Kanda H and Woods G S 1988 *J. Phys. C: Solid State Phys.* **21** 1363
[47] Zaitsev A 2001 *Optical Properties of Diamond—a Data Handbook* (Berlin: Springer)
[48] Collins A T, Thomaz M F and Jorge M I B 1983 *J. Phys. C: Solid State Phys.* **16** 2177
[49] van Oort E 1990 *PhD Thesis* Amsterdam
[50] Reddy N R S, Manson N B and Krausz E R 1987 *J. Lumin.* **38** 46
[51] Martin J P D 1999 *J. Lumin.* **81** 237
[52] Rand S C, Lenef A and Brown S W 1994 *J. Lumin.* **60/61** 739
[53] Lenef A and Rand S C 1996 *Phys. Rev.* B **53** 13441
[54] Lenef A, Brown S W, Redman D A, Rand S C, Shigley J and Fritsch E 1996 *Phys. Rev.* B **53** 13427
[55] Kozankiewicz B, Aloshyna M, Orrit M, Tamarat P, Gudmundsdottir A D and Platz M S 2000 *J. Phys. Chem.* A **104** 7464
[56] Nizovtsev A P, Kilin S Y, Jelezko F, Popa I, Gruber A, Tietz C and Wrachtrup J 2003 *Opt. Spectrosc.* **94** 848
[57] Kurtsiefer C, Mayer S, Zarda P and Weinfurter H 2000 *Phys. Rev. Lett.* **85** 290
[58] Beveratos A, Brouri R, Gacoin T, Poizat J P and Grangier P 2001 *Phys. Rev.* A **64** 061802
[59] Beveratos A, Kuhn S, Brouri R, Gacoin T, Poizat J P and Grangier P 2002 *Eur. Phys. J.* D **18** 191
[60] Rand S C 1994 *Properties and Growth of Diamond* (London: INSPEC) p 235
[61] Jelezko F, Gaebel T, Popa I, Gruber A and Wrachtrup J 2004 *Phys. Rev. Lett.* **92** 076401
[62] Kennedy T A, Colton J S, Butler J E, Linares R C and Doering P J 2003 *Appl. Phys. Lett.* **83** 4190
[63] Hanson R, Witkamp B, Vandersypen L M K, van Beveren L H W, Elzerman J M and Kouwenhoven L P 2003 *Phys. Rev. Lett.* **91** 196802
[64] van der Wiel W G, De Franceschi S, Elzerman J M, Fujisawa T, Tarucha S and Kouwenhoven L P 2003 *Rev. Mod. Phys.* **75** 1
[65] Durkan C and Welland M E 2002 *Appl. Phys. Lett.* **80** 458
[66] Wago K, Botkin D, Yannoni C S and Rugar D 1998 *Phys. Rev.* B **57** 1108
[67] Berman G P and Tsifrinovich V I 2000 *Phys. Rev.* B **61** 3524
[68] Mamin H J, Budakian R, Chui B W and Rugar D 2003 *Phys. Rev. Lett.* **91** 207604
[69] Jelezko F, Gaebel T, Popa I, Domhan M, Gruber A and Wrachtrup J 2004 *Preprint* quant-ph/0402087